

The planetary nebula population of M33 and its metallicity gradient: A look into the galaxy's distant past ¹

Laura Magrini^{1,2}

*Istituto Nazionale di Astrofisica, Osservatorio Astrofisico di Arcetri
Istituto Nazionale di Ottica Applicata, Firenze, I 50125, Italy*

`laura@arcetri.astro.it`

Letizia Stanghellini³

National Optical Astronomy Observatories, Tucson, AZ 85719

`lstanghellini@noao.edu`

and

Eva Villaver^{4,5}

Space Telescope Science Institute, Baltimore, MD 21218

Affiliated with the Hubble Space Telescope Division of the European Space Agency

`villaver@stsci.edu`

ABSTRACT

The Planetary Nebula (PN) population of M33 is studied via multi-fiber spectroscopy with Hectospec at the MMT. In this paper we present the spectra of 102 PNe, whereas plasma diagnostic and chemical abundances were performed on the 93 PNe where the necessary diagnostic lines were measured.

About 20% of the PNe are compatible with being Type I; the rest of the sample is the progeny of an old disk stellar population, with main sequence masses $M < 3M_{\odot}$ and ages $t > 0.3$ Gyr.

By studying the elemental abundances of the PNe in the M33 disk we were able to infer that: (1) there is a tight correlation between O/H and Ne/H, broadly excluding the evolution of oxygen; (2) the average abundances of the α -elements are consistent with those of H II regions, indicating a negligible global enrichment in the disk of M33 from the epoch of the formation of the PN progenitors to the present time; (3) the radial oxygen gradient across the M33 disk has a slope of -0.031 ± 0.013 dex kpc^{-1} , in agreement, within the errors, with the corresponding gradient derived from H II regions. Our observations do not seem to imply that the metallicity gradient across the M33 disk has flattened considerably with time. We report also the discovery of a PN with Wolf-Rayet features, PN039, belonging the class of late [WC] stars

Subject headings: planetary nebulae: general, abundances, individual (M33 system) — galaxies: individual(M33), evolution, abundances

¹Observations reported here were obtained at the MMT Observatory, a joint facility of the Smithsonian Institution and the University of Arizona.

1. Introduction

The galaxy M33 (NGC 598) is one of the closest spiral galaxies of the Local Group. The measured distance to M33 ranges from 730 kpc (Christian

& Schommer 1987) to 910 kpc (Kim et al. 2002), with the most recent estimates of Sarajedini et al. (2006) and Bonanos et al. (2006) in the mid-range. The proximity of M33, together with its large angular size (optical size $53' \times 83'$, Holmberg 1958), and its intermediate inclination ($i=53^\circ$), allows detailed studies of its stellar populations and ionized nebulae.

M33 is a galaxy rich in both PNe and H II regions. The population of PNe in M33 was early investigated using an objective-prism survey by Ford (1983) and Lequeux et al. (1987). The advent of wide-field CCD cameras allowed deeper surveys. Magrini et al. (2000) identified 131 candidate PNe. More recently, Ciardullo et al. (2004) confirmed a large number of previously detected PNe and identified new candidates, leading to the current number of spectroscopically confirmed PNe: 138 in the M33 disk and 2 in its halo.

Due the closeness of M33 and the brightness of the giant H II regions, their spectroscopy was obtained since the 70s. Searle (1971) presented spectrophotometry of eight H II regions, and further spectroscopic studies were carried on by Smith (1975), Kwitter & Aller (1981), and by Vílchez et al. (1988). Several catalogs of the M33 H II regions have been published, such as those by Courtes et al. (1987), Calzetti et al. (1995), Wyder et al. (1997), and Hodge et al. (1999). Recently, the Local Group Census (LGC, Corradi & Magrini 2006) and the Local Group Survey (LGS, Massey et al. 2007) have provided deep narrow- and broad-band ~ 2 square degree coverage of M33, disclosing a conspicuous number of new emission-line objects located at all galactocentric distances.

Given the wealth of information on its PN and H II region populations, M33 is indeed an ideal candidate to test chemical evolution predictions. The aim of the spectroscopic studies of PNe and H II regions is devoted both to the individual studies of these objects, and to draw the radial metallicity gradient across the disk. In particular, PNe and H II regions have two very different formation ages, and the comparison of these two populations provides insight on the evolution of the host galaxy. PN progenitors are low- and intermediate-mass stars (LIMS), with masses between 1 and $8 M_\odot$, which must have been formed between $\sim 3 \times 10^7$ yr and 10 Gyr ago (Maraston

2005). Instead H II regions are very young.

During their evolution, LIMS do not modify, at least at zeroth approximation, the composition of α - elements such as oxygen, neon, argon, and sulfur. These elements are produced mainly from the nucleosynthesis of Type II supernovae and maintain their capability to testify their original presence in the interstellar cloud that gave birth to the PN progenitor. While there are indications that for extremely low metallicities both oxygen and neon could be modified, as it has been observed both in the SMC and in other dwarf galaxies (Leisy and Dennefeld 2006; Magrini et al. 2005; Kniazev et al. 2008), at the metallicity of M33 one does not expect any nucleosynthesis activity involving these elements (Marigo 2001).

On the other hand, the helium, nitrogen, and carbon abundances measured in PNe do not correspond to those at the time of the progenitor's formation, since these elements are synthesized in LIMS. These elements hence give information on LIMS evolution accordingly to their initial mass and metallicity, and, at given metallicity, are helpful to constrain the PN progenitor mass and age.

The M33 metallicity gradient derived from α -element abundances has been the focus of several studies already, both involving PNe and H II regions. The advantage of M33 with respect to our Galaxy, as a playground for gradients, is that PNe in M33 have well determined galactocentric distances (with relative errors within 5%) compared to the large indetermination of Galactic PN distances (Stanghellini et al. 2008). Magrini et al. (2004) using PN spectroscopy in M33 determined the elemental abundances of 11 PNe, and Magrini et al. (2007b) (hereafter M07b) derived an oxygen radial gradient of $\Delta(\text{O}/\text{H}) / \Delta R = -0.11 \pm 0.04$ dex kpc^{-1} , where R is the galactocentric distance. The sample of 11 PNe was too small for a definite answer to the PN gradient of M33, especially given the paucity of PNe observed at large galactocentric distances.

The metallicity gradient of M33 using H II regions has been obtained by many authors, with broadly different results. The first studies by Smith (1975), Kwitter & Aller (1981), and Vílchez et al. (1988) agreed on a steep oxygen gradient. Garnett et al. (1997) also obtained a steep gradient, with $\Delta(\text{O}/\text{H}) / \Delta R = -0.11 \pm 0.02$ dex kpc^{-1} by homogeneously com-

piling published data. Recent determinations, such as those by Crockett et al. (2006), Magrini et al. (2007a), and Rosolowsky et al. (2008) (hereafter M07a and RS08, respectively) seem to converge to a much shallower gradient, respectively deriving $\Delta(\text{O}/\text{H}) / \Delta R = -0.012 \pm 0.011$, -0.054 ± 0.011 , and -0.027 ± 0.012 dex kpc^{-1} . The most recent result by Rubin et al. (2008), based on Ne/H and S/H , gives -0.058 ± 0.014 and -0.052 ± 0.021 dex kpc^{-1} , respectively. The RS08 sample is the largest to date, and should be used preferentially, since the results from small samples might emphasize the scatter rather than the slope.

Metallicity gradients in M33 have also been estimated from young giant stars (Herrero et al. 1994, McCarthy et al. 1995, Venn et al. 1998, Monteverde et al. 1997, 2000, Urbaneja et al. 2005), and from AGB (Cioni et al. 2008), RGB stars (Stephens et al. 2002, Kim et al. 2002, Galletti et al. 2004, Tiede et al. 2004, Brooks et al. 2004, Barker et al. 2006), and Cepheids (Beaulieu et al. 2006).

One of the most discussed questions about the metallicity gradient in disk galaxies is how it evolves with time. Chemical evolution models (see e.g. M07b for a review of M33 models) predict different temporal behaviors of the metallicity gradient depending on assumptions such as gas inflow and outflow rate, and star and cloud formation efficiencies. Observations are needed to constrain these theoretical scenarios, but so far they have been insufficient, especially for the old populations. Comparing different sets of results for the young stellar populations, such as H II regions, and the old population, such as AGB and RGB stars, is also delicate, since the techniques of observing and analyzing nebulae and stars are very different, each with its own collection of uncertainties.

The idea behind the observations leading to this paper is to study the chemical and physical properties of a large number of PNe and H II regions using the same set of observations, the same data reduction and analysis techniques, and identical abundance determination methods, in order to avoid all biases due to the stellar vs. nebular analysis. The chemical properties of PNe and H II regions will provide us with snapshots at two epochs in the life-time of M33, in particular of its metallicity gradient. In the present paper we show the results obtained from the PN data. We have

obtained the first sizable sample of M33 PNe with uniformly derived abundances in order to build the first sound gradient determination from PNe. In a forthcoming paper we will present our own H II region results, and we will compare them with the PN results presented here.

This paper is organized as follows: in § 2 we present the observations and data reduction, in § 3 we discuss the plasma diagnostics used and how we determine the abundances of the PNe, and in § 4 we describe the PN properties. In § 5 we compare the results with the PN populations in other galaxies. The chemical abundance gradients and their implications in the evolution of M 33 are discussed in § 6 and in § 7. Finally in § 8 we summarize our results, and present the conclusions of this work.

2. Observations and data reduction

We obtained spectra of 102 PNe and 48 H II regions in M33 using the MMT Hectospec fiber-fed spectrograph (Fabricant et al. 2005) which is equipped with an Atmospheric Dispersion Corrector. The spectrograph was used with a single setup: 270 mm^{-1} grating at a dispersion of $1.2 \text{ \AA pixel}^{-1}$. The resulting total spectral coverage ranged from approximately 3600 \AA to 9100 \AA , thus including the basic emission-lines necessary for the determination of their physical and chemical properties. The instrument deploys 300 fibers over a 1° diameter field of view and the fiber diameter is $\sim 1.5''$ (6 pc using a distance of 840 kpc to M 33). The 102 PNe were selected from the catalog of Ciardullo et al. (2004), including four new PNe discovered therein at large galactocentric radii.

In Table 1 we present the list of the observed PNe. Column (1) gives the identification number from Ciardullo et al. (2004) except for PNe 153 to 156 which are from LGC observations (Corradi & Magrini 2006); columns (2) and (3) give the equatorial coordinates, RA and DEC at J2000.0, and column (4) gives the $[\text{O III}]$ magnitude from Ciardullo et al. (2004) following the definition by Jacoby (1989).

The H II regions of our sample were chosen either based on their $[\text{O III}]$ brightness, or among those whose chemical abundances had already been measured by others so we can use them as a control sample. In this paper we only use the

TABLE 1
OBSERVED PNE

Id (1)	RA J2000.0 (2)	DEC (3)	M [OIII] (4)
PN001	1:32:09.04	30:22:05.700	23.51
PN002	1:32:26.54	30:25:49.800	23.53
PN003	1:32:38.03	30:24:00.603	21.82

NOTE.—(1) Identification number from Ciardullo et al. (2004), except for PNe 153 to 156, which are from LGC observations (Corradi & Magrini 2006); (2), (3) galactic coordinates at J2000.0; (4) [O III] magnitude following the definition by Jacoby (1989). Table 1 is published in its entirety in the electronic edition of the *Astrophysical Journal*. A portion is shown here for guidance regarding its form and content.

data of the H II regions to test our procedures by comparing our fluxes with those in the literature.

We used a large number of fibers to take sky spectra for sky-subtraction. In order to optimize the sky-subtraction we selected low diffuse-emission areas on the face of M33 from the INT H α and [O III]-continuum frames (Magrini et al. 2000). Since the continuum from the PN central star can not be detected at the M33 distance any continuum emission in the spectra has to be arising from an underlying unresolved stellar population. However, the continuum emission in our spectra is in most cases negligible, and therefore the Balmer absorption lines coming from the stellar background are unimportant.

Five 1800 s exposures were taken on the night of October 13, 2007, and three additional 1800 s exposures of the same field were obtained on November 12, 2007. The airmass during the observations ranged between 1.07 and 1.4 during the night of October 13, and from 1.3 to 1.5 on November 12. The seeing was 1.2'' and 1.7'', respectively. Several dome-flat and sky-flat exposures were obtained during the nights of observations to perform the data reduction. Arc exposures with the calibration lamp He-Ne-Ar were taken for wavelength calibration.

The spectra were reduced using the Hectospec package. All observations were bias subtracted, overscan corrected, and trimmed. The science exposures were flat-fielded and combined together to eliminate cosmic rays, and the one-dimensional spectra were extracted and wavelength calibrated.

The relative flux calibration was done observing the standard star Hiltm600 (Massey et al. 1988) during the nights of October 15 and November 27. The standard star was observed with airmass ~ 1.1 . The emission-line fluxes were measured with the package SPLOT of IRAF². Errors in the fluxes were calculated taking into account the statistical error in the measurement of the fluxes, as well as systematic errors of the flux calibrations, background determination, and sky subtraction.

The observed line fluxes were corrected for the effect of the interstellar extinction using the extinction law of Mathis (1990) with $R_V=3.1$.

We derived $c(\text{H}\beta)$, the logarithmic nebular extinction, by using the weighted average of the observed-to-theoretical Balmer ratios of H α , H γ , and H δ to H β (Osterbrock & Ferland 2006).

Table 2 gives the results of our line measurements and extinction corrections. Column (1) gives the PN name; column (2) gives the nebular extinction coefficient $c(\text{H}\beta)$ with its error; columns (3) and (4) indicate the emitting ion and the rest-frame wavelength in \AA ; columns (5), (6), and (7) give the measured line fluxes (F_λ), their absolute errors ($\Delta(F_\lambda)$, and finally the extinction corrected fluxes (I_λ). Both F_λ and I_λ are normalized to $\text{H}\beta=100$.

In order to confirm the goodness of our spec-

²IRAF is distributed by the National Optical Astronomy Observatory, which is operated by the Association of Universities for Research in Astronomy (AURA) under cooperative agreement with the National Science Foundation

TABLE 2
OBSERVED AND DE-REDDENED FLUXES.

Id (1)	$c(H\beta)$ (2)	Ion (3)	λ (\AA) (4)	F_λ (5)	$\Delta(F_\lambda)$ (6)	I_λ (7)
PN001	0.323 ± 0.026	HI	4340	47.6	3.7	52.4
		HeII	4686	58.0	4.4	60.1
		HI	4861	100.0	4.8	100.0
		[OIII]	4959	304.2	7.4	298.9
		[OIII]	5007	917.8	12.2	894.0
PN002	0.343 ± 0.030	HI	6563	362.2	8.0	289.0
		HI	4340	42.3	3.9	46.9
		HI	4861	100.0	4.8	100.0
		[OIII]	4959	304.1	7.5	298.5
		[OIII]	5007	953.0	12.	927.04
PN003	0.460 ± 0.014	HI	6563	368.3	8.	289.70
		[OII]	3727	101.8	1.6	137.2
		HI	3835	7.7	0.8	10.1
		HeI	3889	9.1	0.8	11.7
		[NeIII]/HI	3968	7.6	0.6	9.6
		HI	4100	17.3	0.8	21.1
		HI	4340	37.5	1.2	43.1
		[OIII]	4363	7.4	0.7	8.5
		HeI	4471	4.4	0.7	4.9
		HI	4861	100.0	1.8	100.0
		[OIII]	4959	178.5	2.0	174.2
		[OIII]	5007	540.1	3.0	520.2
		[NII]	5755	3.7	0.7	3.0
		HeI	5876	22.4	1.0	18.0
		[NII]	6548	43.5	1.0	31.6
		HI	6563	384.8	2.4	280.0
		[NII]	6584	128.2	1.6	92.7
		HeI	6678	5.2	0.7	3.7
		[SII]	6717	7.2	0.6	5.1
		[SII]	6731	10.3	0.8	7.3
HeI	7065	9.7	0.8	6.5		
[ArIII]	7135	14.8	0.8	9.9		

NOTE.—(1) PN name; (2) nebular extinction coefficient $c(H\beta)$ with its error; (3) emitting ion; (4) rest-frame wavelength in \AA ; (5) measured line fluxes; (6) absolute errors on the measured line fluxes; (7) extinction corrected line fluxes. Both F_λ (5) and I_λ (7) are expressed on a scale where $H\beta=100$. Table 2 is published in its entirety in the electronic edition of the *Astrophysical Journal*. A portion is shown here for guidance regarding its form and content.

troscopic calibration we compare our emission-line flux measurements of both H II regions and PNe with previously published fluxes of the same objects. In Figure 1 we plot our measured fluxes against the ones from the literature, where the two dashed lines mark differences of ± 0.15 dex between the two sets. We found a good agreement between the sets, especially for bright emission lines, giving us confidence of a sound spectral calibration.

In Figure 2 we show, as an example of the data quality, the spectra of three PNe with different excitation.

3. Plasma Diagnostics and Abundances

3.1. Electron Densities and Temperatures

We have used the extinction-corrected intensities to obtain the PN electron densities and temperatures. In order to calculate the electronic densities we used the doublet of the sulfur lines [S II] $\lambda\lambda 6716, 6731$, while for the electron temperatures we used the ratios [O III] $\lambda 4363/(\lambda 5007 + \lambda 4959)$ and [N II] $\lambda 5755/(\lambda 6548 + \lambda 6584)$. We performed plasma diagnostics by using the 5-level atom model included in the *nebular* analysis package in IRAF/STSDAS (Shaw & Dufour 1994).

We have also used the standard forbidden line diagnostics IRAF routines in *nebular* to determine the electron temperatures. We have determined the low- and medium-excitation temperatures from the [O III] and the [N II] line ratios, respectively (see also Osterbrock & Ferland 2006, §5.2). The temperature uncertainties have been estimated by formal error propagation of the absolute errors on the line fluxes (see also Table 4). The average relative uncertainties in the determination of $T_e[\text{O III}]$ and $T_e[\text{N II}]$ are of the order of 5% and 15%, respectively.

The [O III] and [N II] temperature diagnostics are available, respectively, for 32 and 8 PNe of our sample. Only for six PNe we can use both temperature diagnostics. In order to improve the size of the PN sample with temperature determinations we looked for correlations between the electron temperature and various diagnostics of the nebular excitation, similarly to the approach followed by Kaler (1986) for a Galactic PN sample.

In Figure 3 we plot the [O III] electron tem-

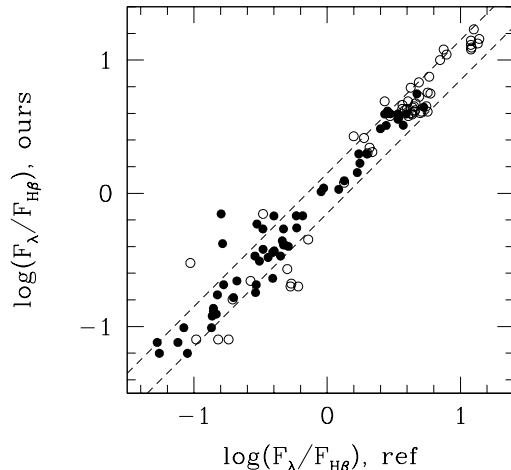


Fig. 1.— Emission-line flux measurements of both H II regions (filled circles) and PNe (empty circles) are compared to previously published fluxes. The fluxes of the H II regions have been taken from Kwitter & Aller (1981); Vilchez et al. (1988); Crockett et al. (2006), M07a; RS08, and the PN ones are from Magrini et al. (2003).

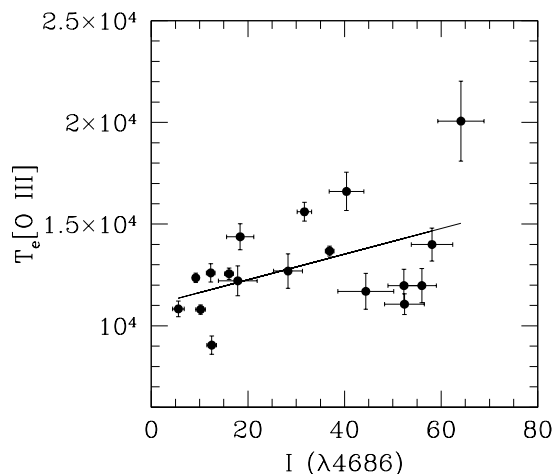


Fig. 3.— [O III] electron temperature vs. $I_{\lambda 4686}$ line intensity, scaled for $I_{H\beta}=100$ and corrected for extinction. The solid line is the fit done with the *fitexy* routine, shown in Eq. (1).

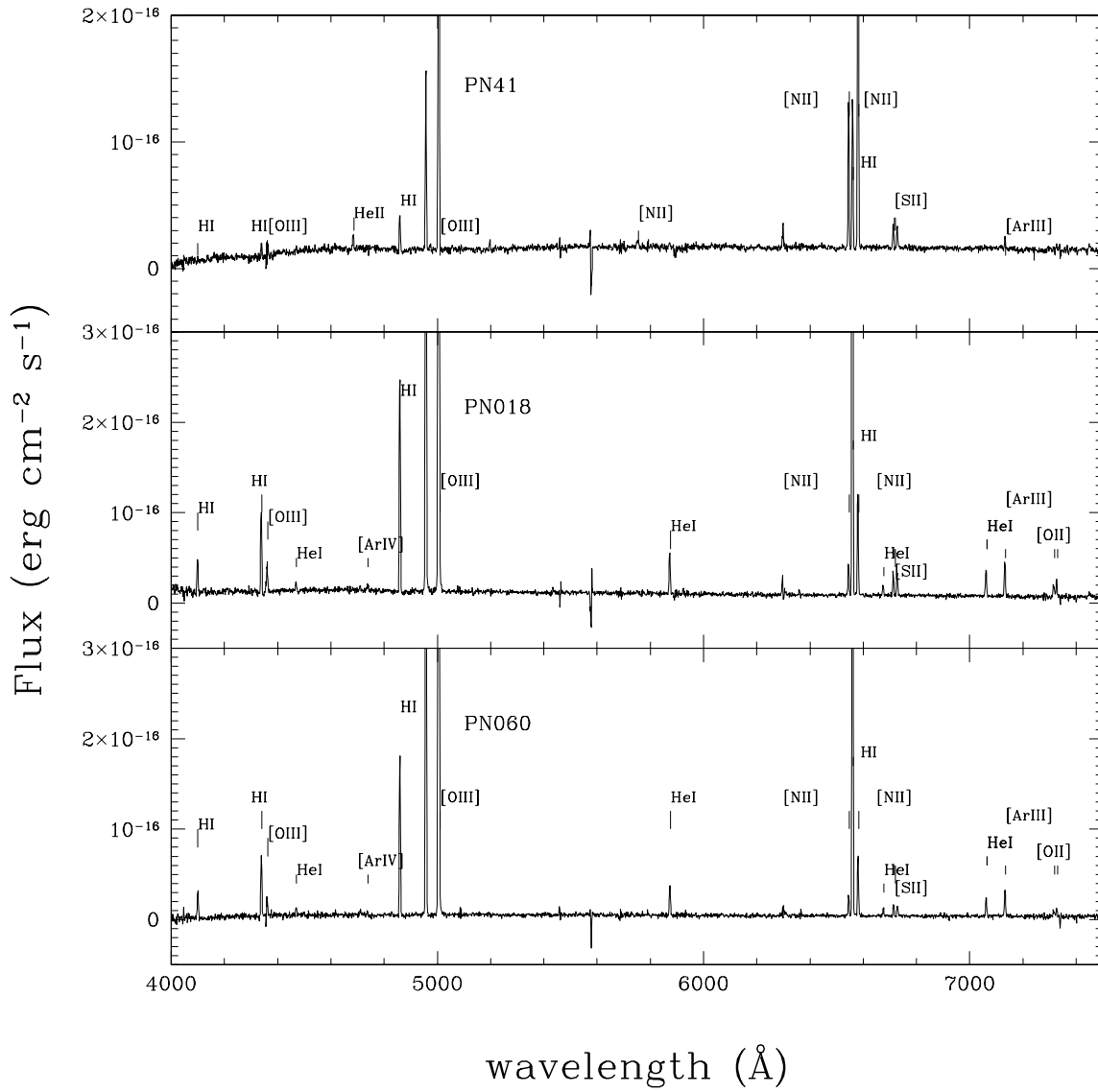


Fig. 2.— Spectra of three PNe with different excitation selected from our sample in order to show the data quality.

perature against the intensity of the $I_{\lambda 4686}$ line, scaled for $I_{H\beta}=100$ and corrected for extinction. Both quantities are plotted with their formal error bars. Planetary nebulae in this plot are those hot enough for helium to be doubly ionized. We find a clear correlation between the [O III] electron temperature and the intensity of the $I_{\lambda 4686}$ line, an effect that is expected as the central stars heat the medium-high excitation nebulae. In order to use this correlation in our temperature calculation we have applied the routine *fitexy* in Numerical Recipes (Press et al. 1992) to fit the relation between the two variables, taking into account their errors, and minimizing χ^2 .

For $I_{\lambda 4686} > 0$ we find:

$$T_e[\text{O III}] = (63 \pm 8) I_{\lambda 4686} + (11,000 \pm 200), \quad (1)$$

where $T_e[\text{O III}]$ is given in K and $I_{\lambda 4686}$ is scaled to $H\beta=100$. Note that using a different fitting routine, such as *sixlin* (Isobe et al. 1990), we determine temperatures that agree with the ones of Eq. (1) at the 1% level. We infer that we are able to estimate the temperatures to better than 10% with the above formulation.

If $I_{\lambda 4686}=0$ we assume a constant value of $T_e[\text{O III}]$, as in Kaler (1986). The average $T_e[\text{O III}]$ for $I_{\lambda 4686}=0$ is 12100 ± 1500 K, which is compatible with the continuity of Eq. (1). Note that both this value and Eq. (1) give temperatures that are consistently higher than those found by Kaler (1986) in Galactic PNe, an effect that is probably due to the lower metallicity that characterizes the M33 stellar populations (see Stanghellini et al. (2003) for a discussion on how metallicity affects the nebular temperatures).

In Figure 4 we show $T_e[\text{N II}]$ against $I_{\lambda 4686}$, where both quantities are plotted with their formal errors. The line represents the mean value of $T_e[\text{N II}] = 13600 \pm 2100$ K, which has been derived using the (inverse squared) relative temperature errors as weights. Once again, while the physical behavior of the temperatures is similar to that found in Kaler (1986), the actual values are higher, possibly reflecting the lower efficiency of the cooling process at low metallicity. For $I_{\lambda 4686} > 0$ we adopt $T_e[\text{N II}] = 13,600$ K.

If $I_{\lambda 4686}=0$, we expect $T_e[\text{N II}]$ to decrease with the stellar temperature. The only way to frame this decline is to use the ratio between the fluxes of the singly-ionized to the doubly-ionized oxygen.

By correlating the oxygen line strengths, corrected for extinction, to the electron temperatures for the PNe with measured [N II] lines we find:

$$T_e[\text{N II}] = (11,700 \pm 2800) - (2800 \pm 4000) \log \frac{I_{\lambda 3727-29}}{I_{\lambda 4959} + I_{\lambda 5007}}. \quad (2)$$

Note that in our spectra the $\lambda\lambda 3727 - 29$ lines are always blended. If the oxygen lines are not available, and $I_{\lambda 4686}=0$ we assume $T_e[\text{N II}] = 14,100 \pm 2800$ K, which, in this case, is the weighted mean of the temperatures.

3.2. Chemical abundances

We computed the ionic abundances using the *nebular* analysis package in IRAF/STSDAS (Shaw & Dufour 1994). The elemental abundances were then determined by applying the ionization correction factors (ICFs) following the prescriptions by Kingsburgh & Barlow (1994) for the case where only optical lines are available. As discussed in the previous §, the [O III] $\lambda 4363$ emission line was measured with a sufficiently high signal to noise ratio in 32 PNe, affording the direct determination of the $T_e[\text{O III}]$. We could also directly measure $T_e[\text{N II}]$ in 8 PNe. For the other targets we adopted the temperatures derived from the relations we have described in the previous Section. In the abundance analysis we have used $T_e[\text{N II}]$ for the calculation of the N^+ , O^+ , S^+ abundances, while $T_e[\text{O III}]$ was used for the abundances of O^{2+} , S^{2+} , Ar^{2+} , He^+ , and He^{2+} .

We calculated the abundances of He I and He II using the equations of Benjamin et al. (1999) in two density regimes, i.e. $n_e > 1000 \text{ cm}^{-3}$ and $\leq 1000 \text{ cm}^{-3}$. The Clegg's collisional populations were taken into account (Clegg 1987). Due to the effect of double collisions not being properly corrected, the He^+/H ionic abundance from the $\lambda 7065$ emission-line is quite different from the ionic abundance computed from $\lambda\lambda 4471$, 5876 , and 6678 . We thus omit the abundance derived from the former line from the average. The computed individual ionic and elemental abundances of each PN are shown in Table 3, where column (1) gives the PN identification name; columns (2) and (3) show the plasma diagnostic and abundances available for each PN, where in column (2) we label each diagnostic, and in column (3) we give the

TABLE 3
PLASMA DIAGNOSTICS AND ABUNDANCES

Id (1)	(2)	(3)
PN001		
	Te(OIII)	14650 ^b
	Te(NII)	13600 ^b
	HeII/H	0.063
	He/H	0.063
	OIII/H	7.586 10 ⁻⁰⁵
	ICF(O)	1.000
	O/H	7.586 10 ⁻⁰⁵
PN002		
	Te(OIII)	14650 ^b
	Te(NII)	13600 ^b
	OIII/H	7.884 10 ⁻⁰⁵
	ICF(O)	1.000
	O/H	7.884 10 ⁻⁰⁵
PN003		
	Te(OIII)	14000 ^a
	Te(NII)	15200 ^a
	Te(OIII)	12060 ^b
	Te(NII)	14120 ^b
	Ne(SII)	2540
	HeI/H	0.125
	He/H	0.125
	OII/H	1.590 10 ⁻⁰⁵
	OIII/H	6.500 10 ⁻⁰⁵
	ICF(O)	1.000
	O/H	8.090 10 ⁻⁰⁵
	NII/H	7.168 10 ⁻⁰⁶
	ICF(N)	5.087
	N/H	3.646 10 ⁻⁰⁵
	ArIII/H	4.47 10 ⁻⁰⁷
	ICF(Ar)	1.245
	Ar/H	8.359 10 ⁻⁰⁷
	SII/H	1.736 10 ⁻⁰⁷
	ICF(S)	1.276
	S/H	1.665 10 ⁻⁰⁶

^acomputed from electron temperature diagnostic lines.

^bderived from the relations in §3.

NOTE.—(1) identification name; (2) label of each plasma diagnostic and abundances available; (3) relative value obtained from our analysis. Table 3 is published in its entirety in the electronic edition of the *Astrophysical Journal*. A portion is shown here for guidance regarding its form and content.

TABLE 4
TYPICAL ERRORS IN DEX

Magnitude (1)	T_e (2)	$\Delta(\text{He}/\text{H})$ (3)	$\Delta(\text{O}/\text{H})$ (4)	$\Delta(\text{N}/\text{H})$ (5)	$\Delta(\text{Ne}/\text{H})$ (6)	$\Delta(\text{Ar}/\text{H})$ (7)	$\Delta(\text{S}/\text{H})$ (8)	N. PNe (9)
20.60-21.00	<i>l</i>	0.03	0.025	0.06	0.05	0.06	0.09	8
	<i>c</i>	-	0.17	0.40	0.43	0.34	0.43	1
21.01-21.50	<i>l</i>	0.04	0.03	0.06	0.06	0.11	0.11	9
	<i>c</i>	0.09	0.20	0.34	0.43	0.30	0.30	8
21.51-22.00	<i>l</i>	0.04	0.03	0.04	0.08	0.09	0.09	5
	<i>c</i>	0.08	0.21	0.34	0.43	0.34	0.30	8
22.01-22.50	<i>l</i>	0.08	0.04	0.07	0.15	0.17	0.11	6
	<i>c</i>	0.11	0.21	0.40	0.43	0.40	0.30	16
22.51-23.00	<i>l</i>	0.13	0.09	0.16	0.16	0.17	0.11	4
	<i>c</i>	0.17	0.20	0.40	0.43	0.43	0.30	9
23.51-24.00	<i>l</i>	0.09	0.07	0.09	0.13	0.18	0.16	1
	<i>c</i>	0.21	0.23	0.40	0.43	0.43	0.30	12
24.01-24.50	<i>c</i>	0.11	0.21	0.34	0.43	0.43	0.43	5
24.51-25.00	<i>c</i>	-	0.45	-	-	-	-	2
25.01-25.50	<i>c</i>	-	0.5	-	-	-	-	1

NOTE.—(1) Magnitude range; (2) method of the electron temperature determination, where *l* means that the temperature has been measured based on an emission line and *c* means that we used the correlations described in §3; (3-8) typical errors in dex of the total abundances; (9) number of PNe available in each bin.

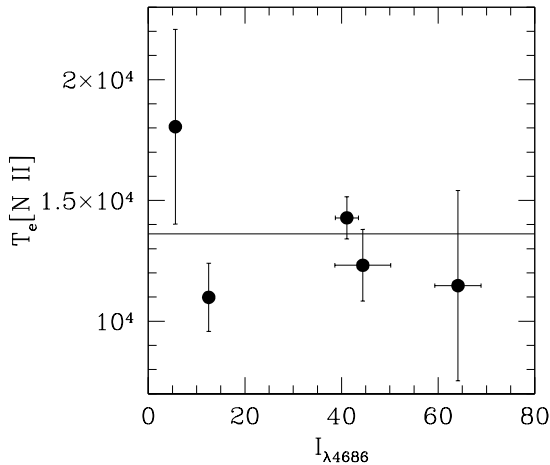


Fig. 4.— Same as Figure 3 but for the $T_e[\text{N II}]$ electron temperature. The solid line represents the mean value of $T_e[\text{N II}] = 13600 \pm 2100$ K, which has been derived using the relative temperature errors as weights.

relative value obtained from our analysis.

The formal errors on the ionic and total abundances were computed taking into account the uncertainties in the observed fluxes, in the electron temperatures and densities, and in $c(\text{H}\beta)$. The errors (in dex) of the final abundances are given in Table 4. Typical errors are given for PNe in different $[\text{O III}]$ magnitude ranges, taking also into account whether the electron temperatures were derived from emission-line diagnostic or from the relations described in § 3.1. In the latter case, we assumed a percentage error on the electron temperature of $\sim 10\%$, which is the dispersion of the relation used to derive the temperature. The first column of Table 4 gives the magnitude range; column (2) gives the method used for the electron temperature determination, where *l* means that the temperature has been measured based on an emission line and *c* means that we used the correlations described in §3; columns (3) to (8) give the typical errors in dex of the total abundances. The last column gives the number of PNe on each bin.

4. The PN population

Most of the PNe discovered in M33 belong to its disk, with only two PNe having radial velocities compatible with the halo population (Ciardullo et

TABLE 5
AVERAGE CHEMICAL ABUNDANCES AND ABUNDANCE RATIOS

Sample (1)	He/H (2)	O/H (10^{-4}) (3)	N/H (10^{-4}) (4)	Ne/H (10^{-5}) (5)	Ar/H (10^{-6}) (6)	S/H (10^{-6}) (7)	N/O (8)	Ne/O (9)
M33 PNe, Disk (91)	0.118±0.074	1.96±1.27	1.09±1.54	4.09±3.08	1.19±0.57	3.34±1.71	0.40±0.32	0.17±0.06
M33 PNe, non-Type I (72)	0.114±0.083	1.73±0.93	0.39±0.19	3.65±2.11	1.12±0.50	4.46±2.30	0.18±0.06	0.17±0.06
M33 PNe, Type I (19)	0.135±0.027	2.70±1.88	1.66±1.88	4.83±4.25	1.38±0.68	6.64±3.80	0.58±0.33	0.16±0.04
M33 PNe, Halo (2)	0.120:	2.62±0.31	0.84:	3.47±0.82	1.24±0.28	6.45:	0.31:	0.13±0.03
M33 HII regions	0.101±0.015(a)	2.04±0.75(b)	1.28±0.57(a)	4.24±2.61(c)	1.31 ±0.45(a)	5.85±2.28(a)	0.06±0.02(a)	0.20±0.06(c)
Solar value(d)	0.085±0.02	4.57±0.04	0.60±0.09	6.9±1.0	1.51±0.30	13.8±2.0	0.13±0.10	0.15±0.05
LMC PNe	0.103±0.026	2.32±1.65	1.48±1.75	4.04±3.60	1.14±0.72	3.46±8.88	0.87±1.15	0.17 ±0.09
SMC PNe	0.113±0.022	1.05±0.46	0.28±0.33	1.77±1.32	0.59±0.59	4.80±6.57	0.28±0.50	0.17 ±0.08
Galactic PNe	0.123±0.042	3.53±1.95	2.44±3.46	9.68±7.98	1.26±1.24	...	0.67±0.82	0.25±0.10

NOTE.—(1) the PN sample; (2-7) average chemical abundances by number with their rms uncertainties; (8-9) $\langle N/O \rangle$ and $\langle Ne/O \rangle$, the average of N/O and Ne/O values for each object.

^aChemical abundances computed using the sample of M07a, extended to all literature data with direct electron temperature measurement.

^bO/H is calculated with the cumulative sample of M07a, which includes also all previous O/H with direct electron temperature measurement, and RS08.

^cNe/H and Ne/O are from Crockett et al. (2006).

^dSolar value from Asplund et al. (2005).

^eValue from a single object.

al. 2004). Therefore, we have the opportunity to analyze in detail a pure disk PN population by excluding from our analysis the two suspected halo PNe (namely PN067 and PN024). We have also excluded from our analysis the PN039 since its physical conditions do not allow us to obtain abundance diagnostics. PN039 has a WR-nucleus and will be discussed in detail in the Appendix.

4.1. The He/H vs N/O diagram

The plot of the N/O ratio vs the He/H one is a classical diagnostic diagram used to discriminate PNe of different types, i.e. with different mass progenitors. The N/O ratio provides information about the stellar nucleosynthesis during the AGB phase of LIMS. On the one hand, nitrogen is produced in AGB stars in two ways: by neutron capture, during the CNO cycle, and by hot-bottom burning. Hot-bottom burning produces primarily nitrogen but occurs only if the base of the convective envelope of the AGB stars is hot enough to favor the conversion of ^{12}C into ^{14}N . Thus nitrogen is expected to be mostly enriched in those PNe with the most massive progenitors, i.e. with turnoff mass larger than $\sim 3 M_{\odot}$ (van der Hoek & Groenewegen 1997; Marigo 2001). The He/H ratio gives also an indication of the initial mass of the progenitor, the nebula is enriched progressively for more massive stars, it reaches a plateau between 3 and $4 M_{\odot}$, and then it increases again toward the higher masses (Marigo 2001).

In order to make a selection of the PNe with high-mass progenitors, in Figure 5, we plot the M33 disk PNe on the He-N/O plane. Peimbert & Torres-Peimbert (1983) found that Galactic PNe that were nitrogen- and helium-enriched also had bipolar shape, and were located closer to the Galactic plane. It looked like these PNe formed a younger population, which they defined as those with $\log(N/O) \geq -0.3$ and $\text{He}/\text{H} \geq \sim 0.125$, and called them Type I PNe. Kingsburgh & Barlow (1994) analyzed a much larger sample and re-define the Galactic Type I PNe as those having $\log(N/O) \geq -0.1$, with 18% of the PNe in their sample being of Type I. Dopita (1991) analyzed LMC PNe and noted that the Type I definition needed a revision to allow for the lower metallicity of the LMC with respect to the Galaxy, setting the limit of Type I PNe to $\log(N/O) \geq -0.5$ for the LMC. Leisy & Dennefeld (2006) basically confirmed this

limit. Magrini et al. (2004) also noted that the definition of Type I PNe depends on the metallicity, because the amount of nitrogen that can be produced by hot bottom burning is dependent on the amount of carbon present, and also because the oxygen abundance depends on the metallicity of the galaxy. Since the oxygen metallicity of M33 is very similar to that of the LMC, we use the Type I limits as in Dopita (1991), namely, Type I PNe are those with $\log(N/O) > -0.5$, independent of helium abundance. With this definition we found 19 PNe being Type I in the disk of M33 ($\sim 20\%$ of the whole disk population) and one in the halo.

4.2. The Ne/H and S/H vs O/H diagrams

The study of the chemical evolution of galaxies needs strong constraints regarding the past composition of the ISM, and PNe can supply them, in particular with their soundly-determined oxygen abundances. The questions is whether oxygen (and neon) is modified in LIMS while in their AGB phase.

A possible way to verify this is to study the relationship between neon and oxygen. These elements derive both from primary nucleosynthesis, mostly in stars with $M > 10 M_{\odot}$. If the O/H and Ne/H abundances are really independent of the evolution of the PN progenitors through the AGB phase, a tight correlation between their abundance should be observed.

In Figure 6 we show O/H against Ne/H for the 55 M33 PNe where both abundances were available. The slope of the correlation is close to unity, 0.90 ± 0.11 , with a correlation coefficient $R_{xy} = 0.81$, pointing at a locked variation of these two elements. Recent results from Wang & Liu (2008) indicate that oxygen and neon could be manufactured with similar yields also in LIMS, but only at very low metallicities, $12 + \log(O/H) < 8$. These results are however still not explained by current nucleosynthesis theories that predict different channels, and thus different yields, for Ne and O production in LIMS at low metallicity (cf., e.g., Karakas & Lattanzio 2003, Marigo et al. 2003). Our findings confirm that in M33, as in LMC, and the Galaxy, there is no evidence of enhancement of oxygen and neon in PNe.

Similar correlations are expected also for sulphur versus oxygen, since sulphur is manufactured

by massive stars. In Figure 7 we plot the sulfur versus oxygen abundances of the 38 M33 PNe where these abundances are available. Their relationship has a slope of 0.97 ± 0.22 and a correlation coefficient of 0.51, showing moderately good correlation. We refrain from showing and analyzing the argon to oxygen relation. As seen in Stanghellini et al. (2006), these quantities might not correlate due to their different origin. Even if both elements are manufactured in massive stars, argon is synthesized in very different α -element processes than oxygen, thus a lockstep of these elements is not completely expected.

5. Comparison of abundances of different stellar populations, and of PN populations of other galaxies

The average chemical abundances of our M33 PNe are reported in Table 5 where the first column describes the selected sample, columns (2) to (7) give the average total abundance of He/H, O/H, Ne/H, Ar/H, and S/H, whereas the last two columns, (8) and (9), give the mean values of N/O and Ne/O. The average abundances were computed excluding those abundances from upper limit detections. When the emission lines for temperature diagnostics were not detected, we adopted the electron temperatures discussed in §3.1. Their larger uncertainties were taken into account by larger formal errors in the total chemical abundances as described in Table 4.

We group the PNe in M33 into four populations: *i*) the whole PN disk population; *ii*) the disk population excluding those PNe which are believed to be Type I; *iii*) the Type I PNe, and *iv*) the halo PN population as classified by Ciardullo et al. (2004). For the sake of comparison we add to the Table the average chemical abundances of the M33 H II regions, the solar abundances, and the average abundances of the PNe in LMC, SMC (Stanghellini 2008) and the Galaxy (Stanghellini et al. 2006). Note, however, that the population of the Type I and non-Type I classes remains somewhat uncertain, since about a dozen PNe could belong to either class based on their formal abundance errors. However, the chemical abundances and distributions of Type I and non-Type I PNe in M33 are very similar, so that the displacement of a few PNe from a group to the other would not

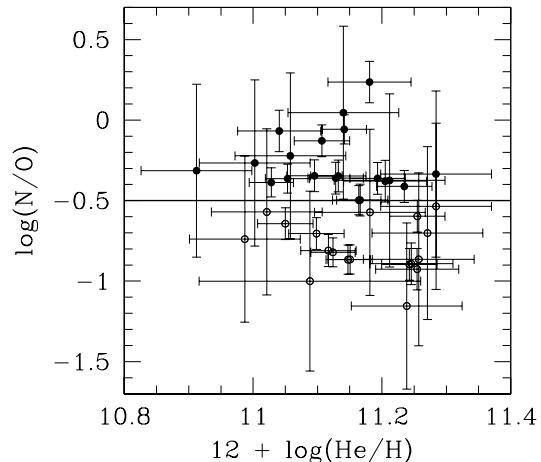


Fig. 5.— $\log(\text{N}/\text{O})$ versus $12 + \log(\text{He}/\text{H})$. Type I PNe and non-type I PNe are plotted as filled circles and empty circles respectively, according to the definition of Dopita (1991). The continuous line mark $\log(\text{N}/\text{O}) > -0.5$ that, independently of helium abundance, defines the area of Type I PNe.

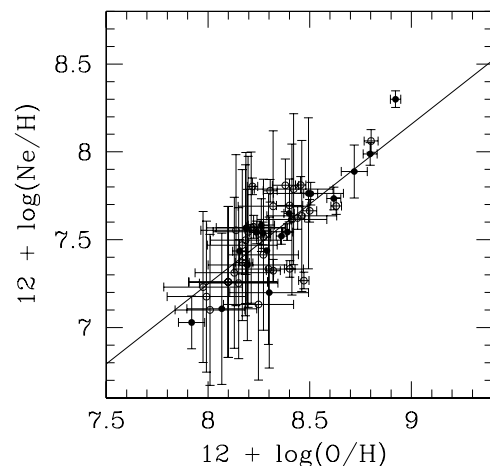


Fig. 6.— The relationship between oxygen and neon abundances. Symbols are as in Figure 5. The continuous line is the weighted least square fit to the complete sample of PNe.

change our results significantly.

An inspection of Table 5 affords several interesting clues on the chemical evolution of galaxies. First, if we compare the average abundances of the α -elements of the M33 disk PNe with those of the H II regions, we do not note significant enrichment in the H II regions, leading to the conclusion that these elements are not substantially modified in the LIMS evolution. We substantially found a flat age-metallicity relationship in M33 all the way to the time of PN formation. Second, we infer that the metallicity of the PNe in M33, based on oxygen abundances, is sub-solar. If we consider the entire sample of disk PNe in M33 we see that the averages of α -elements are virtually identical to those of PNe in the LMC, with PN metallicity about 1/2 that of the Galaxy, and twice the SMC on average, both in oxygen and neon.

From Table 5 we see that the average Ne/O ratio in the general population of M33 PNe is identical to that of the LMC, but lower than the mean Ne/O in Galactic PNe. This finding is right on the mark with the recent results of Wang & Liu (2008). In fact Wang & Liu (2008) found that the Ne/O ratio increases with increasing oxygen metallicity both in PNe and in H II regions. This suggests a different enrichment history of neon and oxygen in the ISM and thus probably different production mechanisms of these two α -elements in massive stars, in agreement with current theoretical calculations by Kobayashi et al. (2006). While we should expect the solar Ne/O ratio to be consistent with that of Galactic disk PNe and H II regions, we note that the Asplund et al.'s (2005) value, as well as Grevesse & Sauval's (1998), is slightly discrepant in this scenario. Both PNe and H II regions in the Galactic disk give a consistent Ne/O ratio of ~ 0.25 , higher than the solar value. Our results on M33 PNe seem thus to be consistent with the recent suggestions of a revision of the solar Ne/O ratio and the absolute neon (e.g. Wang & Liu 2008, Rubin et al. 2008).

The N/O average shown in Table 5 for M33 PNe is lower than the Galactic and higher than the SMC values. The comparison to the LMC average has limited importance, giving the large range of LMC N/O values.

6. The abundance gradients

In Figure 8, we show the oxygen abundance as a function of galactocentric distance for our sample of disk PNe. The galactocentric distances were computed by adopting a distance to M33 840 kpc, as determined by Freedman et al. (1991), an average and well-accepted distance estimate. A weighted linear least-square fit to the complete disk sample gives a gradient:

$$12+\log(\text{O}/\text{H}) = -0.031(\pm 0.013) R_{\text{GC}} + 8.44(\pm 0.06), \quad (3)$$

where R_{GC} is the de-projected galactocentric distance in kpc, computed assuming an inclination of 53° , and a position angle of 22° . In Figures 9, and 10 we plot the radial metallicity gradients of Ne/H and S/H. The solid lines are the weighted linear fits to the complete sample of disk PNe (first row of Table 6 for each element). In all these figures the two symbols refer to Type I (filled circles) or non-Type I (empty circles) PNe.

In Table 6 we show the slopes (column 2) and zero-points (chemical abundances in the centre of the galaxy, column 3) of the metallicity gradients considering different samples of PNe. The sample used and the number of PNe included are given in columns (4) and (5) respectively. For each element, the first row report the gradient obtained considering the whole sample of disk PNe (thus excluding the two possible halo PNe), the second row gives the gradient computed using non-Type I PNe, and the third row gives the gradient obtained for Type I PNe.

The gradients are computed with a weighted least mean square fit. For each element the slope of the three different samples are consistent within the errors. Note that the metallicity gradient of an old stellar population could be affected by the radial migration of stars during cosmic times. The present-time location of a PN could not necessarily be the place where it was born. Radial mixing of stars is believed to be due to several mechanisms, among them the diffusion of stars on their orbits because of various irregularities in the galactic potential (cf. Wielen et al. 1996), to the passage of spiral patterns (cf. Minchev & Quillen 2006), to changes in the angular momentum due to non-asymmetric forces due to molecular clouds

(Spitzer & Schwarzschild 1953). Upper limits to the radial migration rate were estimated by De Simone et al. (2004) and by Haywood (2008), giving similar values around $1.5\text{-}3.7 \text{ kpc Gyr}^{-1}$, limited to a radial region $\pm 2 \text{ kpc}$ from the birth place. The model of Sellwood & Binney (2002) show that spiral waves in galaxy disks churn both the interstellar medium and the stars, affecting their metallicity gradients. The effect of stirring of the entire disk due to the spiral waves is a flattening of the metallicity gradient.

However, the fact that metallicity gradients survive and are well observed in disk galaxies seem to indicate that the effectiveness of the migration processes is moderate.

7. Discussion

The metallicity gradient of PNe allows to analyze how was the metal distribution in the past epochs of M33. In M33 we have the possibility to compare the metallicity gradient of PNe with a good number of other measurements of abundance gradients, in particular from H II regions. The advantage of comparing PNe to H II regions is the similarity of their emission-line spectra in spite of their different evolutionary states that allows to use the same observation techniques, analysis, and abundance determinations.

In order to compare our PN results with the leading samples of M33 H II regions we build the largest, most reliable sample available to date. As already noted by e.g. RS08 and M07a, the size and quality of the sample is fundamental to derive reliable metallicity gradients. In H II regions there is a substantial intrinsic scatter of 0.11 dex in the metallicity at any given distance from the M33 center, which imposes a fundamental limit on the accuracy of gradient measurements that rely on small samples of objects (RS08). Also, in the past, only giant H II regions have been studied, and those might have a steeper metallicity gradient than small and compact H II regions.

We have re-calculated the H II regions metallicity gradients considering a cumulative sample, including that by RS08, consisting of 61 H II regions with accurate abundance determinations, and that by M07a that included new and literature spectroscopy performed to a set of 28 H II regions. The cumulative sample of 89 H II regions gives,

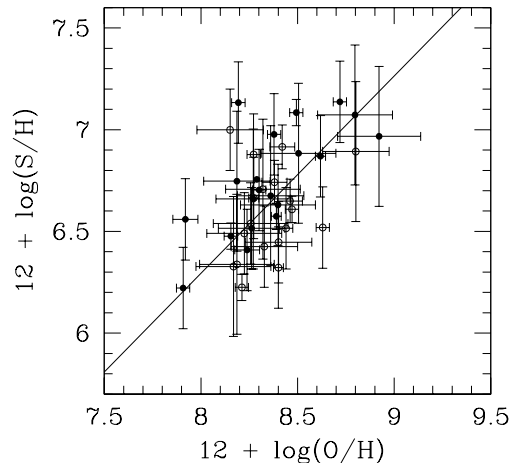


Fig. 7.— The relationship between oxygen and sulphur abundances. Symbols are as in Figure 5. The continuous line is the weighted least square fit to the complete sample of PNe.

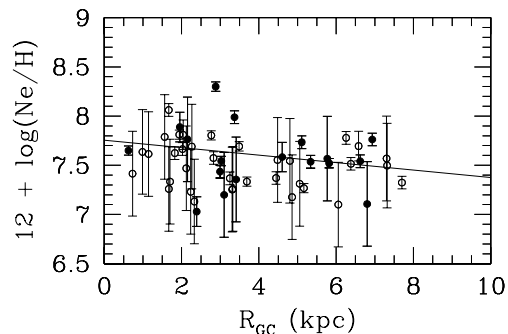


Fig. 9.— The radial gradient of neon abundance. Symbols are as in Fig. 5. The continuous line is the weighted least square fit to the complete sample of disk PNe. Slopes and zero-points are shown in Table 6.

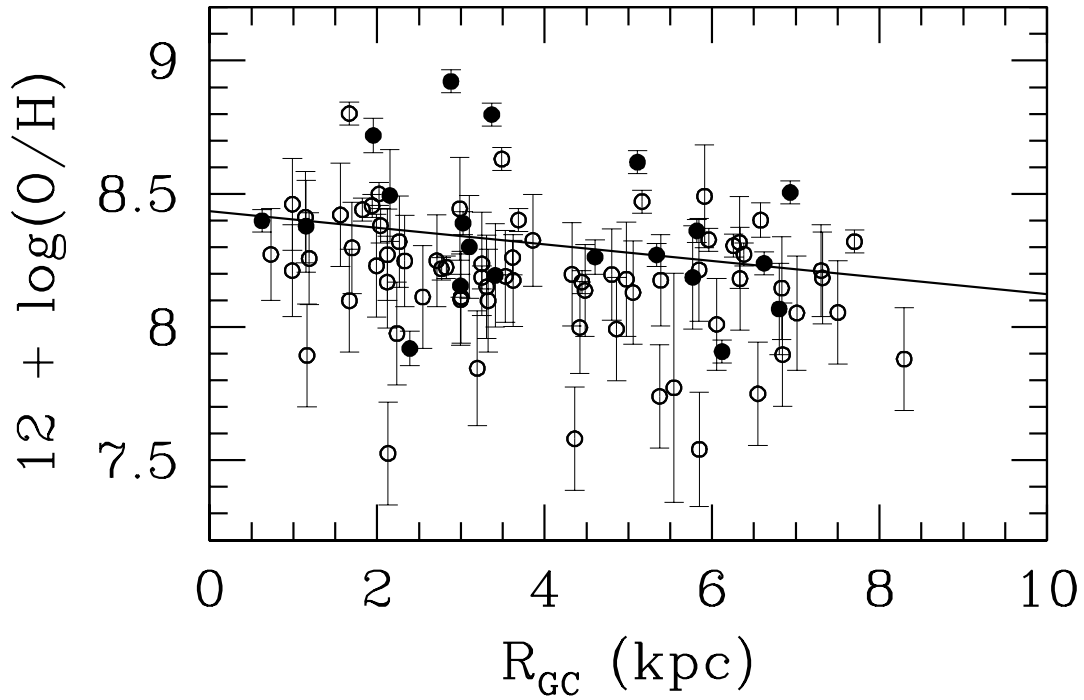


Fig. 8.— The radial gradient of oxygen abundance. Symbols are as in Fig. 5. The continuous line is the weighted least square fit to the complete sample of disk PNe. Slopes and zero-points are shown in Table 6.

TABLE 6
CHEMICAL ABUNDANCE GRADIENTS

Element (1)	Slope (2)	Zero (3)	sample (4)	# PNe (5)
O/H	-0.031 ± 0.013	8.44 ± 0.06	All PNe	91
O/H	-0.030 ± 0.013	8.41 ± 0.06	non-type I PNe	72
O/H	-0.039 ± 0.033	8.56 ± 0.15	type I PNe	19
Ne/H	-0.037 ± 0.018	7.75 ± 0.07	All PNe	55
Ne/H	-0.051 ± 0.019	7.76 ± 0.08	non-type I PNe	37
Ne/H	-0.025 ± 0.037	7.76 ± 0.17	type I PNe	18
S/H	-0.033 ± 0.019	6.77 ± 0.08	All PNe	38
S/H	-0.027 ± 0.020	6.67 ± 0.09	non-type I PNe	19
S/H	-0.041 ± 0.031	6.87 ± 0.14	type I PNe	19

NOTE.—(1) The chemical element for which the gradient is computed; (2) slope of the abundance gradient; (3) zero-point (chemical abundances in the centre of the galaxy); (4) sample of PNe; (5) number of PNe in each sample. For each element, the first row report the gradient obtained considering the whole sample of disk PNe (thus excluding the two possible halo PNe), the second row gives the gradient computed using non-Type I PNe, and the third row gives the gradient obtained of Type I PNe.

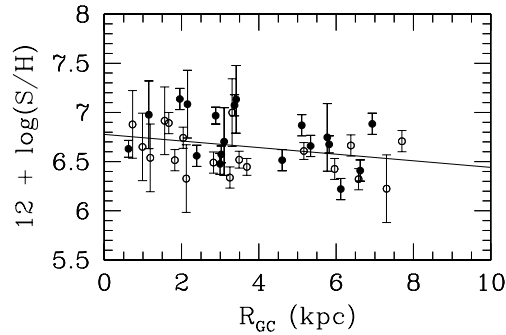


Fig. 10.— The radial gradient of sulphur abundance. Symbols are as in Fig. 5. The continuous line is the weighted least square fit to the complete sample of disk PNe. Slopes and zero-points are shown in Table 6.

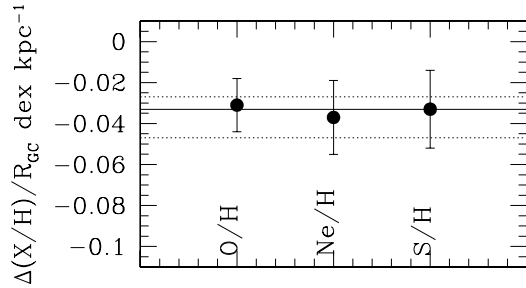


Fig. 11.— The slopes of the radial elemental gradients in M33. The continuous line is the weighted average slope, and the two dashed line give the rms σ of this value.

$$12+\log(\text{O}/\text{H}) = -0.032(\pm 0.009) \times R_{\text{GC}} + 8.41(\pm 0.04). \quad (4)$$

When compared to the best gradient determined using M33 PNe (Eq. 3), we confirm that these gradients are consistent within the errors. We infer that the metallicity gradient of M33 has not changed from the epoch of the formation of the PN progenitors to the present time.

We can use for comparison the gradient of the best measured element, oxygen, or the weighed average of the slope of O/H, Ne/H, and S/H gradient, and shown in Fig. 11, $-0.033 \pm 0.003 \text{ dex kpc}^{-1}$.

In Table 8 we compare our metallicity gradient with the literature values derived using different stellar populations. α -element and iron-peak gradients are separated by a double horizontal line since their different origin (SNII vs. SNIa) suspects a different metallicity distribution through the disk and possibly a different gradient. In each group, α -elements or Fe/H, gradients are ordered by the increasing age of the corresponding stellar population. We considered only metallicity gradients computed with a statically significant sample, thus, e.g., excluding the metallicity gradient with Cepheid stars (Beaulieu et al. 2006).

It is remarkable that both the oxygen and neon metallicity gradients of M33 do not change within the errors even considering populations of different ages, though they are slightly different, the neon gradient having a slightly steeper slope.

In the following we discuss which evolutionary scenario and chemical evolution models are excluded or favored by our results.

The first chemical evolution model attempting to describe the evolution of M33 was that by Diaz & Tosi (1984). Their model assumes a constant and uniform infall rate and fails to reproduce the metallicity gradient observed in M33. Other models that describe the origin and evolution of metallicity gradients are listed in Table 7, where we report the Reference (column 1), the model type (column 2), the resulting oxygen gradient (column 3), and its variation with time (column 4), where a plus sign indicates a flattening of the metallicity gradient with time.

The first three models listed in Table 7 are a family of multiphase models, differing mainly from

the origin and rate of the infalling material. A multiphase model considers the galaxy divided in two or more zones, typically the halo and the disk, composed by baryonic material in different phases: diffuse gas, clouds, stars, and stellar remnants. These models evolve with time (see e.g. Ferrini et al. 1992, 1994 for a complete description), and are characterized by a flattening of the radial metal distribution with time, due to the inside-out formation of the disk.

Mollá et al. (1997) specifically analyzed the time-evolution of the metallicity gradient in several spiral galaxies, where the disk is formed by the primordial gas of the spheroidal protogalaxy which collapses onto the galactic plane and forms out the disk. For M33 they obtained that $\Delta(\text{O}/\text{H})/\Delta(R) \sim -0.21 \text{ dex kpc}^{-1}$, flattening with time at a rate of $+0.005 \text{ dex kpc}^{-1} \text{ Gyr}^{-1}$.

Mollá & Diaz (2005) applied their results to M33 and found metallicity gradients similar to those by Mollá et al. (1997). Gradient evolution is not computed explicitly, but a clear flattening of the gradient is evident in their figures.

M07b built the so-called "accretion" model reproducing the slow formation of the disk of M33 from the inflow of intergalactic gas, which predicts $\Delta(\text{O}/\text{H})/\Delta(R) \sim -0.067 \text{ dex kpc}^{-1}$, also flattening with time at a rate of $+0.003 \text{ dex kpc}^{-1} \text{ Gyr}^{-1}$.

Other types of models, such as those by Chiappini et al. (1997, 2001), were not applied directly to M33, but are notable since they predict steepening of the metallicity gradients with time. These models assume two main accretion episodes for the formation of the galaxy, the first forming the halo, the bulge, and the thick disk in a short timescale, and the second forming the thin disk, with a timescale that is an increasing function of the galactocentric distance. Different assumptions on the star formation threshold and on the timescales of the infall episodes produce the gradients slopes and evolutions reported in Table 7 (see Chiappini et al. 2001 for a detailed description). Note that the behavior of Model D is different from the other models by the same authors in that the assumed slower formation of the outer halo does not influence the disk formation, resulting in steeper gradients.

If for example we assume that the age of all PNe is 5 Gyr, then according to the models by

Molla et al. we would expect a PN gradient which is $-0.025 \text{ dex kpc}^{-1}$ steeper than that of the H II regions. Using the M07b models for the same PNe age, the PN gradient is $-0.015 \text{ dex kpc}^{-1}$ steeper than that of the H II regions. On the other hand, with Models A, B, C by Chiappini et al. (2001) we would observe PN gradients that are flatter than those of H II regions by $+0.04$, $+0.02$, $+0.03 \text{ dex kpc}^{-1}$ respectively. These variations could be even larger for older PN populations. In summary, only the models by M07b, and model B by Chiappini et al. (2001), are marginally consistent with the observations.

To match the small metallicity gradient variation with time we observed with the models of M33 we could invoke a lower accretion rate from the ISM than that used in the M07b models. The resulting simulation should produce a flat metallicity gradient, and a small slope variation in the last 8-10 Gyr, as observed. Detailed analysis of galactic chemical evolution models are out of the scope of this work.

8. Summary and conclusions

We present spectroscopic observations of a large sample (102) of PNe in the spiral galaxy M33. The observations were secured with the spectrograph Hectospec on the 6.5 m telescope MMT.

For 32 PNe the electron temperature was directly computed. Empirical relationships among electron temperatures and bright emission lines as He II $\lambda 4686$, and [O II] $\lambda 3727$ were used to derive electron temperatures of the remaining PNe.

Abundance diagnostic diagrams were built to study the PN population. From the plot of N/O versus He/H we found that the PNe that fulfill the Dopita (1991) definition of Type I PN are 19. Most PNe are non Type I, implying a population mainly composed by PNe from old progenitors, with $<3M_{\odot}$ and ages $>0.3 \text{ Gyr}$.

A tight relationship between the O/H and Ne/H abundances was found, excluding the modification of both elements by PNe progenitors and ensuring oxygen to be a good tracer of the galaxy metallicity.

The average chemical abundances of the PNe were compared to the PN population of the LMC, the SMC, and the Galaxy. Generally speaking, the elemental abundances of the α -elements of the

PNe in the disk of M33 are very similar to those of the LMC. The comparison between M33 PNe and H II regions indicates a negligible global enrichment of the M33 disk from the epoch of the formation of the PN progenitors to the present time.

The radial metallicity gradients of those elements which are not modified during the lifetime of LIMS— oxygen, neon, sulphur— were derived. The best measured element, oxygen, has a slope $-0.031 (\pm 0.013) \text{ dex kpc}^{-1}$ in agreement within the errors with the same gradient derived from H II regions $-0.032 (\pm 0.009) \text{ dex kpc}^{-1}$.

Since the metallicity gradients of PNe and H II regions are practically indiscernible and the mean abundances of the PN and H II region populations are very close, we conclude that the chemical enrichment in M33 from the time of the formation of the PN progenitors to the present-time has been nearly negligible.

TABLE 7
CHEMICAL EVOLUTION MODELS OF M33

Ref.	Model	$\Delta(\text{O}/\text{H})/\Delta(\text{R})$ (present time) (dex kpc ⁻¹)	$(\Delta(\text{O}/\text{H})/\Delta(\text{R}))/\Delta(t)$ (dex kpc ⁻¹ Gyr ⁻¹)
(1)	(2)	(3)	(4)
Mollá et al. (1997)	multiphase, infall from collapse of the halo	-0.21	+0.005
Mollá & Diaz (2005)	multiphase, infall from collapse of the halo	-0.20	...
M07b	multiphase, accretion model	-0.067	+0.003
Chiappini et al.(2001)	model A	-0.065	-0.008
	model B	-0.045	-0.004
	model C	-0.070	-0.006
	model D	-0.20	+0.05

NOTE.—(1) Reference; (2) main characteristics of the chemical evolution model; (3) slope of the present-time O/H radial gradient; (4) time variation of the O/H gradient.

TABLE 8
A SAMPLE OF LITERATURE ABUNDANCE GRADIENTS

Element	Gradient	Population	Age	#	Ref.
(1)	(2)	(3)	(4)	(5)	(6)
O/H	-0.05±0.025	B giants	few Myr	30	Urbaneja et al. (2005)
O/H	-0.032±0.009	H II regions	few Myr	89	RS08 + M07a
O/H	-0.039±0.033	young PNe	<0.3 Gyr	19	this paper
O/H	-0.031±0.013	All PNe	<10 Gyr	91	this paper
O/H	-0.030±0.013	old PNe	0.3-10 Gyr	72	this paper
Ne/H	-0.05±0.02	H II regions	few Myr	30	Willner & Nelson-Patel (2002)
Ne/H	-0.058±0.014	H II regions	few Myr	25	Rubin et al. (2008)
Ne/H	-0.025±0.037	young PNe	<0.3 Gyr	18	this paper
Ne/H	-0.037±0.018	All PNe	<10 Gyr	55	this paper
Ne/H	-0.051±0.019	old PNe	0.3-10 Gyr	37	this paper
Fe/H	-0.06	AGB	~4-6 Gyr	-	Cioni et al. (2008)
Fe/H	-0.04±0.02	RGB	>8 Gyr	-	Kim et al. (2002)
Fe/H	-0.06±0.01	RGB	>8 Gyr	-	Tiede et al. (2004)

NOTE.—(1) Chemical element; (2) slope of the radial gradient with its error; (3) stellar population; (4) typical age of the stellar population; (5) size of the sample; (6) reference.

A. PN039: a planetary nebula with a [WC]-nucleus

PN039 has a WR central star. Its spectrum shows prominent and wide features of He II at λ 4686, 4541, 5411 and of He I at λ 4471, 5876, 6678, 7065. In addition other stellar lines of [CIII] at λ 4056 and 4649, and [CII] at 7107 and 7124 were detected. The FWHM of these lines is 15\AA , to be compared instrumental resolution of about 6\AA . Thus, following the classification of Acker & Neiner (2003) PN039 has a late-type [WC]-9 or [WC]-10 nucleus due to the presence of very bright [CIII] and [CII] lines respect to the [CIV] lines.

The ratio of the sulphur doublet indicates a low density limit $\lesssim 100\text{ cm}^{-3}$, and [O III], 4363/5007 ratio is completely anomalous for a normal PN, giving an electron temperature $\sim 30,000\text{ K}$. The reddening of the nebula is null, within the errors, indicating a little presence of dust.

Acknowledgments: We thank an anonymous referee for his/her valuable comments and suggestions that have improved the paper. We thank D. Fabricant for making Hectospec available to the community and the TAC for awarding us the observing time. We thank the Hectospec instrument team and MMT staff for their expert help in preparing and carrying out the Hectospec observing runs. We thank N. Caldwell, D. Ming and their team for the help during the data reduction. Thanks to Katia Cunha for enlightening scientific discussion, and Richard Shaw for his help with the *nebular* package.

Facilities: Hectospec (MMT).

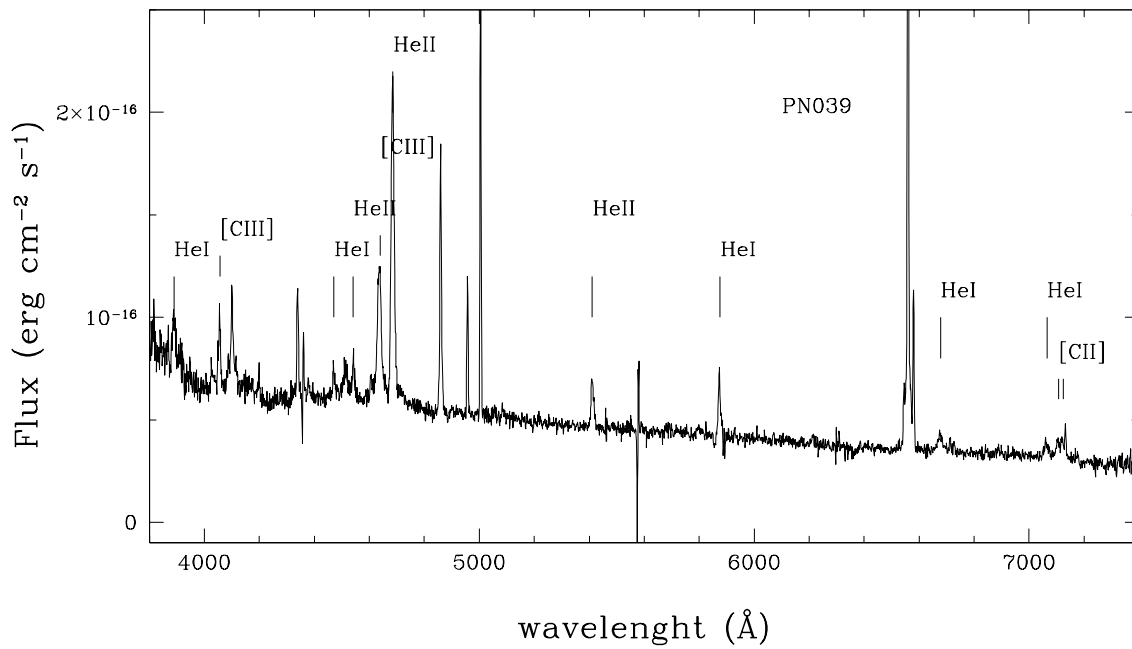


Fig. 12.— The spectrum of PN039 with its [WC] features.

REFERENCES

- Acker, A., Neiner, C. 2003, *A&A*, 403, 659
- Asplund, M., Grevesse, N., Sauval, A. J. 2005, *ASPC*, 336, 25
- Barker, M. K., Sarajedini, A., Geisler, D., Harding, P., Schommer, R. 2006, *AJin press*, astro-ph/0611892
- Beaulieu, J. -P., Buchler, J. R., Marquette, J. -B., Hartman, J. D., Schwarzenberg-Czerny, A., 2006, *ApJ*, 653, 101
- Benjamin, R. A., Skillman, E. D., Smits, D. P., 1999, *ApJ*, 514, 307
- Bonanos, A. Z., et al. 2006, *ApJ*, 652, 313
- Brooks, R. S., Wilson, C. D., Harris, W. E. 2004, *AJ*, 128, 237
- Calzetti, D., Kinney, A. L., Ford, H., Doggett, J., Long, K. S. 1995, *AJ*, 110, 2739
- Chiappini, C., Matteucci, F., & Gratton, R. 1997, *ApJ*, 477, 765
- Chiappini, C., Matteucci, F., & Romano, D. 2001, *ApJ*, 554, 1044
- Christian, C. A., & Schommer, R. A. 1987, *AJ*, 93, 557
- Ciardullo, R., Durrell, P. R., Laychak, M. B., Herrmann, K. A., Moody, K., Jacoby, G. H., Feldmeier, J. J., 2004, *ApJ*, 614, 167
- Cioni, M.-R. L., Irwin, M., Ferguson, A. M. N., McConnachie, A., Conn, B. C., Huxor, A., Ibata, R., Lewis, G., Tanvir, N., 2008, *A&A*, 487, 131
- Clegg, R. E. S., 1987, *MNRAS*, 229, 31
- Corradi, R. L. M., Magrini, L., 2006, in *Planetary Nebulae Beyond the Milky Way*, *ESO Astrophysics Symposia*, 36
- Courtes, G., Petit, H., Petit, M., Sivan, J.-P., Dodonov, S. 1987, *A&A*, 174, 28
- Crockett, N. R., Garnett, D. R., Massey, P., Jacoby, G. 2006, *ApJ*, 637, 741
- Davidge, T. J. 2003, *AJ*, 125, 304
- De Simone, R., Wu, X., Tremaine, S. 2004, *MNRAS*, 350, 627
- Devereux, N., Duric, N., Scowen, P. A. 1997, *AJ*, 113, 236
- Diaz, A. I., & Tosi, M. 1984, *MNRAS*, 208, 365
- Dopita, M. A. 1991, *IAUS*, 148, 393
- Fabricant, D., et al. 2005, *PASP*, 117, 1411
- Ferrini, F., Matteucci, F., Pardi, C., & Penco, U. 1992, *ApJ*, 387, 138
- Ferrini, F., Molla, M., Pardi, M. C., & Diaz, A. I. 1994, *ApJ*, 427, 745
- Freedman, W. L., Wilson, C. D.; Madore, B. F. 1991, *ApJ*, 372, 455
- Ford, H. C., 1983, in *Planetary nebulae; Proceedings of the Symposium*, Dordrecht, D. Reidel Publishing Co., 1983, p. 443-460
- Galletti, S., Bellazzini, M., Ferraro, F., 2004, *A&A*, 423, 925
- Garnett, D. R., Shields, G. A., Skillman, E. D., Sagan, S. P., Dufour, R. J. 1997, *ApJ*, 489, 63
- Grevesse, N., Sauval, A. J. 1998, *Space Science Reviews*, v. 85, Issue 1/2, p. 161-174
- Haywood, M. 2008, *MNRAS*, 388, 1175
- Herrero, A., Lennon, D. J., Vilchez, J. M., Kudritzki, R. P., Humphreys, R. H. 1994, *A&A*, 287, 885
- Hodge, P. W., Balsley, J., Wyder, T. K., Skelton, B. P., 1999, *PASP*, 111, 685
- Holmberg, E., 1958, *Lund Medd. Astron. Obs. Ser. II*, 136, 1
- Kaler, J. B., 1986, *ApJ*, 308, 322
- Karakas, A., Lattanzio, J.C., 2003, *Publ. Astron. Soc. Austr.* 20, 393
- Kim, M., Kim, E., Lee, M. G., Sarajedini, A., Geisler, D. 2002, *AJ*, 123, 244
- Kingsburgh, R. L., Barlow, M. J., 1994, *MNRAS*, 271, 257
- Kniazev, A. Y., et al. 2008, *MNRAS*, 388, 1667

- Kobayashi, C., Umeda, H., Nomoto, K., Tomonaga, N., Ohkuo, T, 2006, ApJ, 653, 1145
- Kwitter, K. B., Aller, L. H., 1981 MNRAS, 195, 939
- Jacoby, J. H., 1989, ApJ, 339, 39
- Isobe, T., Feigelson, E. D., Akritas, M. G., & Babu, G. J. 1990, ApJ, 364, 104
- Leisy, P., Dennefeld, M. 2006, A&A, 456, 451
- Lequeux, J., Meyssonnier, N., Azzopardi, M., 1987, A&AS, 67, 169
- Magrini, L., Corradi, R. L. M., Mampaso, A., Perinotto, M. 2000, A&A, 355, 713
- Magrini, L., Perinotto, M., Corradi, R. L. M., Mampaso, A. 2003, A&A, 400, 511
- Magrini, L., Perinotto, M., Mampaso, A., Corradi, R. L. M. 2004, A&A, 426, 779
- Magrini, L., Leisy, P., Corradi, R. L. M., Perinotto, M., Mampaso, A., & Vilchez, J. M. 2005, A&A, 443, 115
- Magrini, L., Vilchez, J. M., Mampaso, A., Corradi, R. L. M., Leisy, P, 2007a, A&A, 470, 865 (M07a)
- Magrini, L., Corbelli, E., Galli, D. 2007b, A&A, 470, 843 (M07b)
- Maraston, C. 2005, MNRAS, 362, 799
- Marigo, P., 2001, A&A, 370, 194
- Marigo, P., Bernard-Salas J., et al. 2003, A&A, 409, 619
- Massey, P., Strobel, K., Barnes, J. V., Anderson, E., 1988, ApJ, 328, 315
- Massey, P., Olsen, K. A. G., Hodge, P. W., Jacoby, G. H., McNeill, R. T., Smith, R. C., Strong, S. B., 2007, AJ, 133, 2393
- Mathis, J. S., 1990, ARA&A, 28, 37
- McCarthy, J. K., Lennon, D. J., Venn, K. A., Kudritzki, R.-P. 1995, ApJ, 455, 135
- Minchev, I., Quillen, A. C. 2006. MNRAS, 368, 623
- Mollá, M., Ferrini, F., & Diaz, A. I. 1997, ApJ, 475, 519
- Mollá, M., & Díaz, A. I. 2005, MNRAS, 358, 521
- Monteverde, M. I., Herrero, A., Lennon, D. J., Kudritzki, R.-P. 1997, ApJ, 474, 107
- Monteverde, M. I., Herrero, A., Lennon, D. J. 2000, ApJ, 545, 813
- Osterbrock, D. E., Ferland, G. J. 2006, *Astrophysics of Gaseous Nebulae and Active Galactic Nuclei* 2nd. ed. by D.E. Osterbrock and G.J. Ferland. Sausalito, CA: University Science Books, Sky and Telescope, Vol. 78
- Peimbert, M., Torres-Peimbert, S., 1983, in Proceedings of the Symposium, Dordrecht, D. Reidel Publishing Co., 1983, p. 233-241
- Press, W. H., Teukolsky S. A., Vetterling W.T., Flannery, B.F., Numerical Recipes in FORTRAN: The art of scientific computing. 2nd ed. (1992)
- Rosolowsky, E., Simon, J. D., 2008, ApJ, 675, 1213
- Rubin, R.H. et al., 2008, MNRAS, 387, 45
- Sarajedini, A., Barker, M. K.; Geisler, D., Harding, P. Schommer, R., 2006, AJ, 132, 1361
- Searle, L., 1971, ApJ, 168, 327
- Sellwood, J. A., Binney, J. J 2002, MNRAS, 336, 785
- Shaw, R. A., Dufour, R. J, 1994, ASPC, 61, 327
- Smith, H. E. 1975, ApJ, 199, 591
- Spitzer, L., Jr., Schwarzschild, M. 1953, ApJ, 118, 106
- Stanghellini, L., Villaver, E., Shaw, R., Mutchler, M. 2003, ApJ, 598, 1000
- Stanghellini, L., Guerrero, M. A., Cunha, K., Manchado, A., Villaver, E., 2006, ApJ, 651, 898
- Stanghellini, L., 2008, in IAU Symp. 256, in press
- Stephens, A. W., Frogel, J. A. 2002 AJ, 124, 2023
- Tiede, G. P., Sarajedini, A., Barker, M. K. 2004 AJ, 128, 224

- Urbaneja, M. A., Herrero, A., Kudritzki, R.-P., Najarro, F., Smartt, S. J., Puls, J., Lennon, D. J., Corral, L. J. 2005, *ApJ*, 635, 311
- van den Hoek, L. B., Groenewegen, M. A. T., 1997, *A&AS*, 123, 305
- Venn, K. A., McCarthy, J. K., Lennon, D. J., Kudritzki, R. P. 1998 *ASPC*, 147, 54
- Vílchez, J. M., Pagel, B. E. J., Diaz, A. I., Terlevich, E., Edmunds, M. G., 1988 *MNRAS*, 235, 633
- Wang, W., Liu, X.-W., 2008, *MNRAS*, 389, 33
- Wielen, R., Fuchs, B., Dettbarn, C. 1996 *A&A*, 314, 438
- Willner, S. P., Nelson-Patel, K. 2002, *ApJ*, 598, 679
- Wyder, T. K., Hodge, P. W., Skelton, B. P. 1997, *PASP*, 109, 927